Nonlinear Processes in Geophysics (1995) 2: 61 - 79

Nonlinear Processes in Geophysics

Dynamical segmentation and rupture patterns in a "toy" slider-block model for earthquakes

J. B. Rundle[1] and W. Klein[2]

[1] Department of Geology and CIRES, University of Colorado, Boulder, CO 80309, USA
[2] Polymer Center and Department of Physics, Boston University, Boston, MA 02215, USA

Received 7 November 1994 - Accepted 6 April 1995 - Communicated by D. L. Turcotte

Abstract. Lattice models for earthquakes have been shown to capture some of the dynamical properties possessed by natural fault systems. These properties include: 1) a scaling (power law) region in the curve representing event frequency as a function of magnitude and area; and 2) space-time clustering of events. To understand the physical origin of these and other effects, we examine the simplest kind of "toy" slider block model. We obtain results indicating that this model displays several additional kinds of phenomena seen in real earthquake faults, even though "realistic" physics is missing from the model. Asperity-like slip distributions in this model arise from strong elastic coupling, rather than the spatially heterogeneous frictional strength often inferred for real faults. Simulation results indicate that "characteristic" earthquakes can be produced as a consequence of the nonlinear dynamics. Thus segmentation on faults may be a result of the nonlinear dynamics as well as being due to geometric properties of fault systems. These conclusions may be modified when more "realistic" physics is added to the model, although the presence of dynamical effects in the toy model calculations similar to those observed in nature demonstates alternative possibilities for the origin of these effects.

1 Introduction

Understanding the physics of earthquakes is complicated by the fact that the large events of greatest interest recurr at a given location along an active fault only on time scales of the order of hundreds of years (e.g., Richter, 1958; Kanamori, 1983; Pacheco et al., 1992). To acquire an adequate data base of similar large earthquakes therefore requires the use of historical records, which are known to possess considerable uncertainty. Moreover, instrumental coverage of even relatively recent events is often inconsistent, and network coverage and detection levels can change with time (Haberman, 1982). Understanding the details of the rupture process is further complicated by the spatial heterogenity of elastic properties, the vagaries of near field instrumental coverage, and other factors (see for example Heaton, 1990; Kanamori, 1993). We are therefore motivated to use methods that provide insight into details of the rupture process which are complementary to the usual observational techniques (e.g., Kanamori, 1993).

For many problems in statistical mechanics, numerical simulation is the only only practical means of obtaining experimental information about the behavior of a nonlinear system (Binder, 1979; Binder, 1984; Mouritsen, 1984; Ma, 1985; Yeomans, 1992). Numerical simulation has been used extensively to study earthquakes in the recent past (Rundle, 1988, 1989; Rundle & Klein, 1989; Carlson and Langer, 1989; Bak and Tang, 1989; Rundle & Turcotte, 1993; Sahimi et al., 1993). In the case of earthquake faults, the long time scales involved, comparable to the human lifetime, and the (at present) unpredictable nature of the events make earthquakes difficult to study systematically in the field. For this reason, it is most advantageous to develop simulation techniques so that the physics of earthquakes can be studied easily in the computer.

In developing numerical simulation techniques, there are several issues that arise. The first is the use of massless cellular automaton models, instead of models with mass, whose dynamics must be obtained by solving a set of coupled differential equations. The original Burridge-Knopoff model (Burridge and Knopoff, 1967) and its CA successors (Rundle and Jackson, 1977) were not motivated by a first principles derivation, but only as an approximation to a fault. Moreover, the relative importance of inertia in the rupture process, which is responsible for generating seismic radiation, is still not clear. Kanamori and Anderson (1975) estimated that the seismic efficiency η, which measures the fraction of energy in the earthquake lost to seismic radiation, is less than 5%-10%. CA models are in fact dynamical maps, which are known to have a fundamental connection to the dynamics generated by the associated differential equations (Smale, 1967; Arrowsmith and Place, 1990). Finally, it was shown by Nakanishi (1990) that massless CA's can be constructed that give the same quantitative results as the massive slider block models examined by Carlson and Langer (1989). These results include not only the rupture patterns, but also the scaling statistics. There is also clearly a time evolution process in the CA, with a separation of loader plate and source time scales, just as in models with inertia. The physical interpretation of the CA time scales is discussed by Gabrielov et al. (1994). To

Correspondence to: J. B. Rundle

summarize, this issue of the presence or absence of inertia has been examined in the literature and shown to have little significance.

In every simulation, massive or massless, there are a series of fundamental approximations. For example, faults are usually assumed to be planar; boundary conditions might be periodic, or fixed at the ends; interactions between fault segments might be nearest neighbor, $1/r^3$, or long range of some other variety. Friction might be simple stick slip (Mohr-Coulomb); have simple but unrealistic velocity dependence as in the original Burridge-Knopoff model; be based on overly idealized laboratory friction experiments on clean, dry, dust-free sliding surfaces; ignore the effects of pore water; or ignore effects associated with variable normal stress on the fault. All of these various models have their advantages and disadvantages, their adherents and opponents.

In this paper we use the simplest possible model, which we term a "toy" model. There are several important reasons for studying such a toy model. Any dynamical model, which includes both differential equations as well as maps, gives rise to an observed dynamical behavior as a consequence of the physical nature of the model. It is of fundamental interest to ask what minimal set of physics must the model possess in order to demonstrate dynamical effects that are seen in nature. We are therefore making a fundamental distinction between models that previous experience tells us are 'realistic', and 'minimal' models which nevertheless demonstrate important similarities to natural phenomena. The toy model that we examine in this paper is of the latter category. One expects 'realistic' models to match natural fault dynamics well.

The true value of the toy model lies exactly in the somewhat surprising fact that a significant body of natural phenomena are reproduced by the dynamics, including both scaling of earthquake distributions, and as demonstrated here, 'asperities'. This fact leads to the important conclusion that the observed phenomena may either have several origins, or that the true origin is not in the physics included in the more 'realistic' model. In short, the objective of this paper is to ask the question, how little physics can one include in a model and still get interesting, unexpected results? For example, massless cellular automaton slider block models obtain the same kinds of scaling distributions for earthquakes as do massive models which possess inertia. Moreover, neither massive nor massless models include elastic waves, attenuation, viscoelasticity, etc. The logical question is then to what extent the presence of inertia, waves, and so forth play any role in the scaling properties of the phenomena. Another example, which is a major subject of this paper, is that massless slider block models with a uniform failure (strength) threshold can reproduce much of the phenomena usually cited as evidence for the asperity model for earthquakes (Lay et al., 1982). Asperities are usually thought to be associated with a spatially heterogeneous failure threshold, but the results obtained here raise questions about the true physical origin of these phenomena.

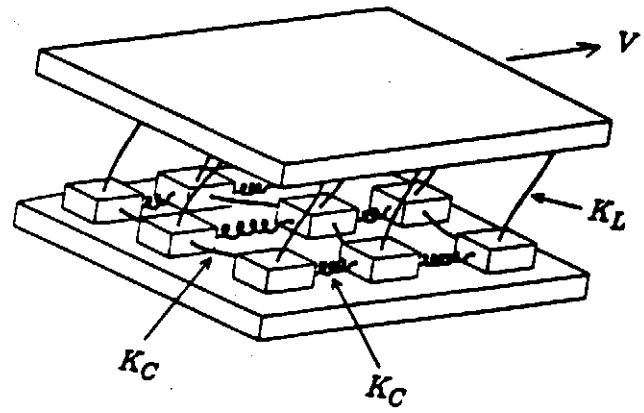

Fig. 1. Picture of the two-dimensional slider block model.

The toy model we use here has been introduced elsewhere (Rundle, 1977; Narkounskaia et al., 1992; Olami et al., 1992). Other papers have focused on examining the scaling properties of the model and establishing its universality class (Narkounskaia et al., 1992; Rundle et al., 1994). Here we explore the phenomenology of the model, beginning with a short description of the model, then give a graphical display of a series of representative results. We compare these to observed data from seismology. In general, one obtains Heaton-type pulses (Heaton, 1990) rather than crack-like solutions (Kostrov, 1964), because healing takes place immediately after a block slides, rather than at a delayed time after slip everwhere is complete.

2 Model

The model used here has been described elsewhere (Rundle and Jackson, 1977). It consists of a massless cellular automaton (CA) version of the model originally proposed by Burridge and Knopoff (1967; see figure 1). Later versions of this model have been proposed by, among others, Nakanishi (1991), Brown et al. (1991), Narkounskaia et al. (1992) and Olami et al. (1992). In this model, a network of massless blocks sliding on a frictional surface are connected to nearest neighbor blocks by coupling springs with spring constant K_C. A loader spring with spring constant K_L connects each block to a loader plate moving with a velocity V, increasing the force on each block at a steady rate. In the original BK model with massive blocks, the frictional force has a velocity dependence that produces lower stress with increased sliding velocity. Once a static force threshold σ^F is equaled or

exceeded, the full inertial equations of motion are solved in the BK model to obtain the slip of each block.

The solution of coupled differential equations makes the simulation of systems with large numbers of elements extremely difficult. Moreover, it is important to simulate as large a system as possible to eliminate the effects of the finite size of the lattice. By contrast, the CA approach for these systems can be made far more computationally efficient since only simple algorithms are used. In slider block models, eliminating the mass in turn eliminates the possiblity of waves and radiation damping. If the seismic efficiency is low, of the order of 5%-10% as is generally assumed (e.g., Kanamori and Anderson, 1975), a case can be made that inertia is less important than other entropic and internal energy effects.

Only the simplest kind of stick-slip friction is used in our CA model. "Clusters" or avalanches of failed blocks can appear because an initially unstable block increases the force on its neighbor blocks as a result of the coupling springs, thereby inducing instability in its neighbors. Each of the clusters of failed blocks represents an earthquake in the simulation. The energy functional for the system of blocks and springs is:

$$H = (1/2)\,\Sigma_i \{ K_L (s_i - Vt)^2 + (1/2)\, K_C\, \Sigma_j [s_j - s_i]^2 \} \qquad (1)$$

In (1), s_i represents the total slip of block i, V is the loader plate velocity, t is time, and the sum over j is carried out over the blocks that are nearest neighbors to block i. The sum over j excludes site i, and the factor (1/2) corrects for the double counting of site i . Equation (1) can be written as:

$$H = (1/2)\,\Sigma_i \{ K_L (s_i - Vt)^2 + K_C\, \Sigma_j [(s_j - Vt) - (s_i - Vt)]^2 \} = (1/2)\,\Sigma_i \{ K_L \phi_i^2 + K_C\, \Sigma_j [\phi_j - \phi_i]^2 \} \qquad (2)$$

where $\phi_i = s_i - Vt$ is the negative of the slip deficit of block i.

The force σ_i (or stress if unit area is assumed) on block i is :

$$\sigma_i = -\partial H / \partial \phi_i = -\{ K_L \phi_i + K_C\, \Sigma_j [\phi_j - \phi_i] \} \qquad (3)$$

A rule that generates evolution through time must be specified, this being the friction law. For the simulations here, we adopt the Mohr-Coulomb law with a spatially constant static failure threshold σ^F , and a spatially constant residual stress σ^R. Upon slip, when $\sigma_i \geq \sigma^F$, each block jumps forward a distance $\Delta s_i = (\sigma_i - \sigma^R) / K_T$, $K_T = K_L + 4K_C$, whereupon it sticks (heals). Different Monte Carlo prescriptions have been used in other realizations of the model (Rundle et al., 1994). The statistical distributions obtained as well as qualitative properties of the results are independent of the time evolution rule used, suggesting that there may be some universal aspects of the phenomena.

The energy functional (1) for a slider block model can be formally obtained from the expression for the energy change due to slip on a planar fault surface in an infinite elastic medium. The expression for the energy contained within an elastic medium due to quasistatic slip on the fault surface S is:

$$H_{EL} = -\int_S d^2\mathbf{x} \{ p(\mathbf{x})\, s(\mathbf{x},t) + 1/2 \int_S d^2\mathbf{x}'\, T(\mathbf{x}-\mathbf{x}')\ \ s(\mathbf{x},t))\, s(\mathbf{x}',t)) \} \qquad (4)$$

The important assumptions are: 1) the constant applied stress field $p(\mathbf{x}) = 0$; 2) a shift to a moving reference system, so that slip s is replaced by slip deficit ϕ; and 3) the Green's function $T(\mathbf{x} - \mathbf{x}')$ falls off sufficiently rapidly as $| \mathbf{r} | = | \mathbf{x}-\mathbf{x}' |$ increases. This last assumption implies that the system (earth) is not ideally elastic, and that there is some infrared "cutoff". In fact, the earth is not ideally elastic, inasmuch as wave attenuation, material creep, plasticity, fluid flow, and other processes are important in fault zones and throughout the lithosphere. The issue of whether there exists an infrared cutoff is equivalent to the problem of whether the elastic interaction is screened by competing interactions due to defects in the solid (Ma, 1985). An example of a Green's function with an infrared cutoff is the asymptotic form $e^{-\alpha r} / r^3$, rather than $1/r^3$, the form appropriate to a perfectly elastic solid. We discuss below the effect a nonzero screening parameter α has on the value of K_C / K_L.

Using a gradient expansion (Ma, 1976) of $\phi(\mathbf{x}',t')$ around $\mathbf{x}$, retaining terms up to the second derivative in $\mathbf{x}$, and integrating by parts, the local interaction energy H_{EL}^{loc} is obtained:

$$H_{EL} \approx H_{EL}^{loc} \equiv 1/2 \int_S d^2\mathbf{x}\ \{ k_L \phi^2(\mathbf{x},t) + k_C (\nabla \phi(\mathbf{x},t))^2 \} \qquad (5)$$

where the spring constant densities k_L and k_C are related to the Green's function by:

$$k_L \equiv -\int_S T(\mathbf{r})\, d^2\mathbf{r} \qquad (-\,0^{th} \text{ moment of T}) \qquad (6)$$

$$k_C \equiv 1/2 \int_S T(\mathbf{r})\, r^2\, d^2\mathbf{r} \qquad (2^{nd} \text{ moment of T}) \qquad (7)$$

To obtain the slider block energy, (5) is spatially coarse grained by averaging the integrand over squares of side length a. Then $\phi(\mathbf{x}) \rightarrow \phi_i$, and noting that $\nabla\phi(\mathbf{x}) \approx (\phi_i - \phi_j)/a$, the slider block energy (2) is obtained. In energy

functionals like (5), k_C is the "range of interaction", and k_L is the "mass" (e.g., Ma, 1976, 1985; Amit, 1984; Yeomans, 1992).

Finally, it should be pointed out that some authors prefer models with considerably more physical detail, specifically with infinite range interactions and a five-parameter friction law (e.g., Ben Zion and Rice, 1993). While that approach has advantages, it has the disadvantages that 1) infinite range interactions means always having to deal with boundary conditions and finite size effects, and 2) it is often difficult to identify the physical origin of various phenomena. Our approach is to begin with as simple a model as possible (minimal model) and progressively add more levels of detail as the effects of the different parameters are clarified.

Since a major concern at present is computational and analytic simplicity, we use a slider-block CA model with spatially constant failure threshold σ^F and residual stress σ^R to simulate seismicity on a fault. The effect of randomness in the model is examined elsewhere (Rundle et al., 1995a,b). The time evolution of the CA model is generated by a jump rule giving the position of the block as a function of the state of stress on the block. The jump rule for the i^{th} block is given by:

$$s_i(t+1) = s_i(t) + J(\sigma_i)\,\Theta(\sigma_i - \sigma^F) \qquad (8)$$

where $\Theta(x)$ is a Heaviside step. The the jump function $J(\sigma_i)$ is

$$J(\sigma_i) = (\sigma_i - \sigma^R) / (K_L + 4K_C) \qquad (9)$$

In the work described in this paper, the simulations were started with the blocks having random initial positions, on lattices of 100 x 100 blocks. The calculations proceed as follows:

1. The loader plate was moved (updated) until the stress on the least stable block reached threshold ($\sigma_i = \sigma^F$).
2. The position of the least stable block is adjusted using (8) - (9).
3. A "Monte Carlo" sweep (iteration) through the entire network (lattice) is carried out and the stress on each block is calculated using equation (3).
4. The position of all blocks at or above threshold ($\sigma_i \geq \sigma^F$) are simultaneously adjusted according to (8) - (9).
5. Further sweeps and block position adjustments are carried out until all of the blocks are in states with $\sigma_i \leq \sigma^F$.
6. The loader plate position is again updated according to step 1.

The time evolution process described in steps 1 - 6 is contained in the equations (3), (8), (9). This model is a V $\rightarrow$ 0 model, because the loader plate moves so slowly that there can only be one initiator block in each avalanche cluster of failed sites (Rundle et al., 1995a). This is the same basic model described by Narkounskaia et al. (1992) and Olami et al. (1992). Growing avalanche clusters will never coalesce into larger clusters, so that each cluster in this (nearest neighbor) model grows outward from only one site. This is evidently an important distinction among various slider block models (Rundle et al., 1995a) with respect to scaling exponents and limit cycle behavior.

3 Simulation results

A fundamental question is whether even such a simple model as the one described here can display effects presently thought to be characteristic of real faults. Specifically, we ask whether "asperity - like" features and "characteristic earthquakes" emerge from these models, even though these features are not put into the model "by hand". If these features are present in the simplest models, the presence of these effects in more realistic detailed models cannot therefore be taken as evidence of the importance of these details. Examples of such details includes realistic fault geometries, crustal structures, inelastic earth rheologies, or heterogeneous frictional strength distributions.

The results of our simulations are shown in figures 2 - 11. In these calculations, a spatially constant threshold $\sigma^F = 350$ was used, together with a spatially constant residual stress $\sigma^R = 10$. Values used for spring constants were $K_C = 1$ (always), and $K_L = 1$ or $K_L = .04$ (as noted in the figure captions and described below). The objective was to examine the extent to which changes in only one parameter, the coupling ratio K_C / K_L, can determine the fundamental phenomenology of the dynamical process. In all cases, simulations were begun from random initial conditions, then the models were run for at least several hundred thousand events to eliminate transients before data were obtained.

Fig. 2 shows simulated earthquake statistics for 20,000 events in a model with $K_C / K_L = 1$. In these and subsequent figures, the seismic moment M_O for an avalanche of failed blocks is defined as:

$$M_O = K_L \sum_{\text{(all failed blocks)}} \{\text{slip}\}$$
$$= K_L \text{ (average slip) (total area)} \qquad (10)$$

The summation is carried out over all failed blocks in the avalanche. Magnitude M is defined by:

$$M = \text{Log}_{10}\{M_O\} \qquad (11)$$

The top left corner plot of figure 2 shows M as a function of time, where time is defined as the position of the loader plate. The apparent horizontal solid lines in the lower portion of the plot are in reality individual dots representing, from the bottom, the one-block events, next the two-block events, and so forth, until at higher

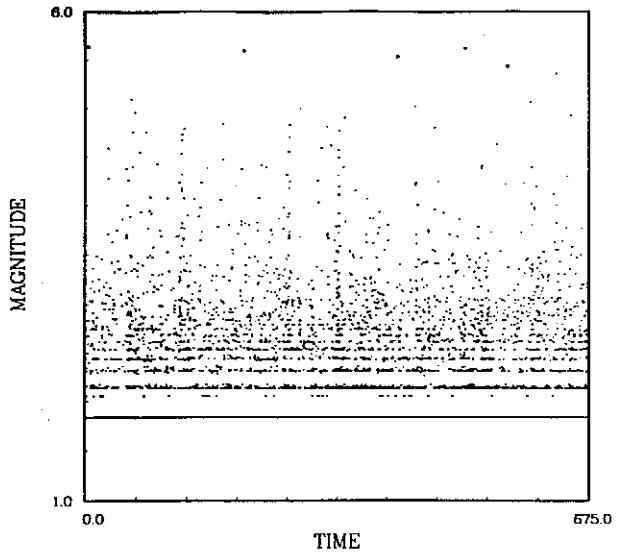

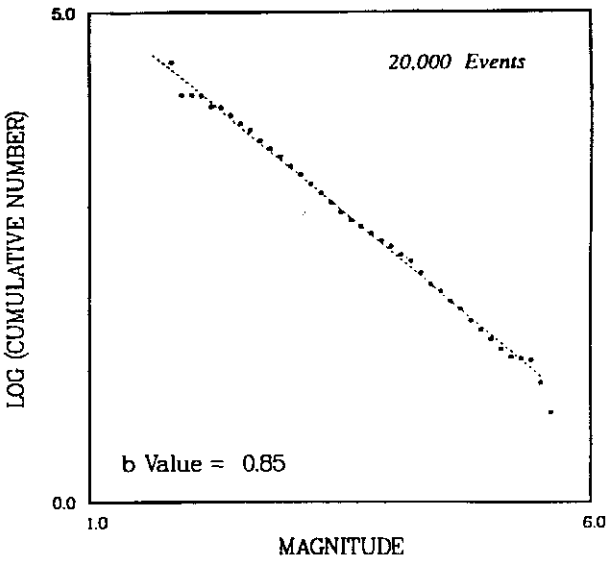

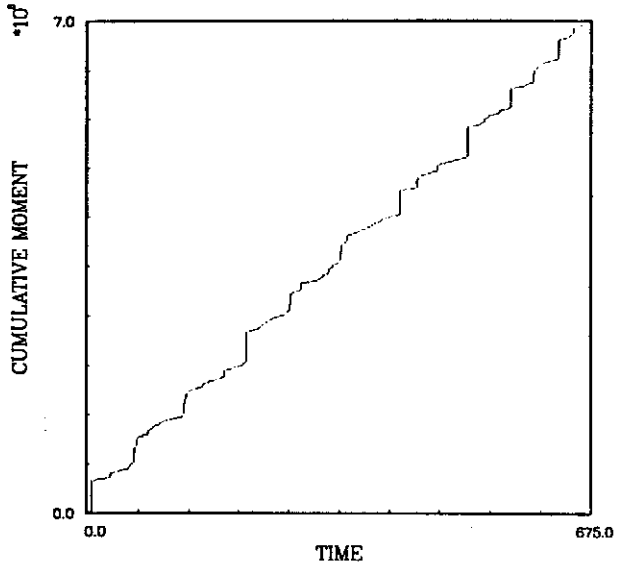

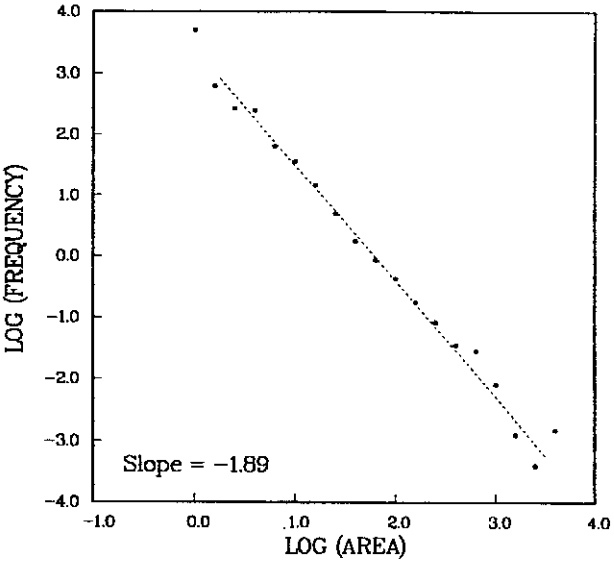

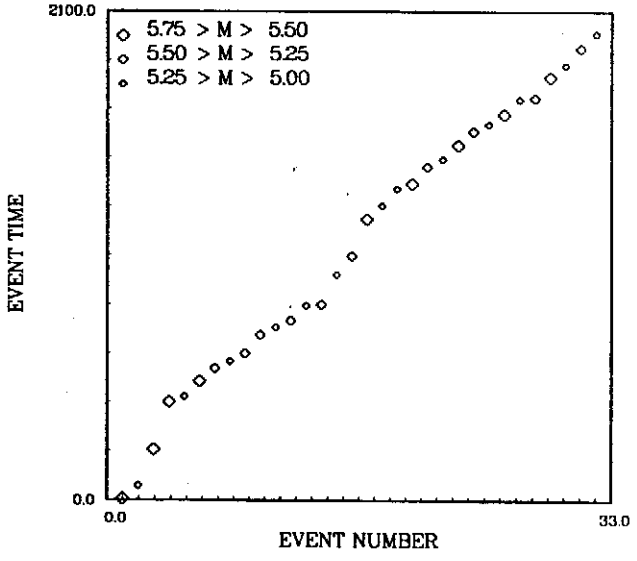

Fig. 2. Results from simulation with $K_C / K_L = 1$, $K_L = 1$. (a) Top left is magnitude-time plot of synthetic events, with magnitude as defined in the text. (b) Middle left is cumulative moment-time plot. (c) Bottom left is event time plotted against sequence number for the largest events shown in (a) and (b). (d) Top right is cumulative magnitude-frequency relation for all events. Note that b-value of .85 should not be compared with Gutenberg-Richter values for real data since magnitude is defined as Log10 (moment). (e) Probability density for frequency of occurrence plotted against area of event. Note that slope of -1.89 is close to the slope of -2 for real data, and is independent of assumptions about constants in the magnitude-frequency relation.

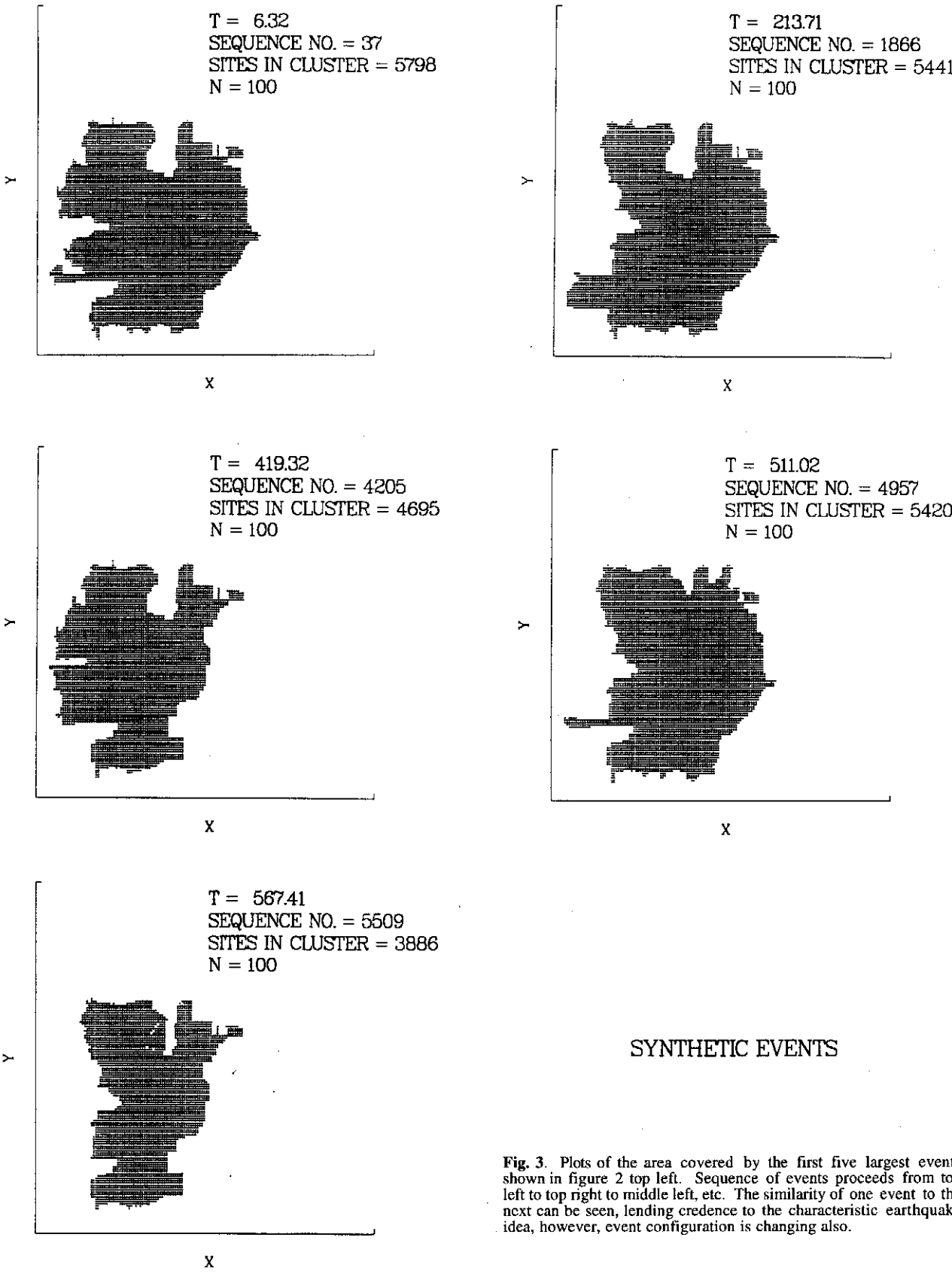

Fig. 3. Plots of the area covered by the first five largest events shown in figure 2 top left. Sequence of events proceeds from top left to top right to middle left, etc. The similarity of one event to the next can be seen, lending credence to the characteristic earthquake idea, however, event configuration is changing also.

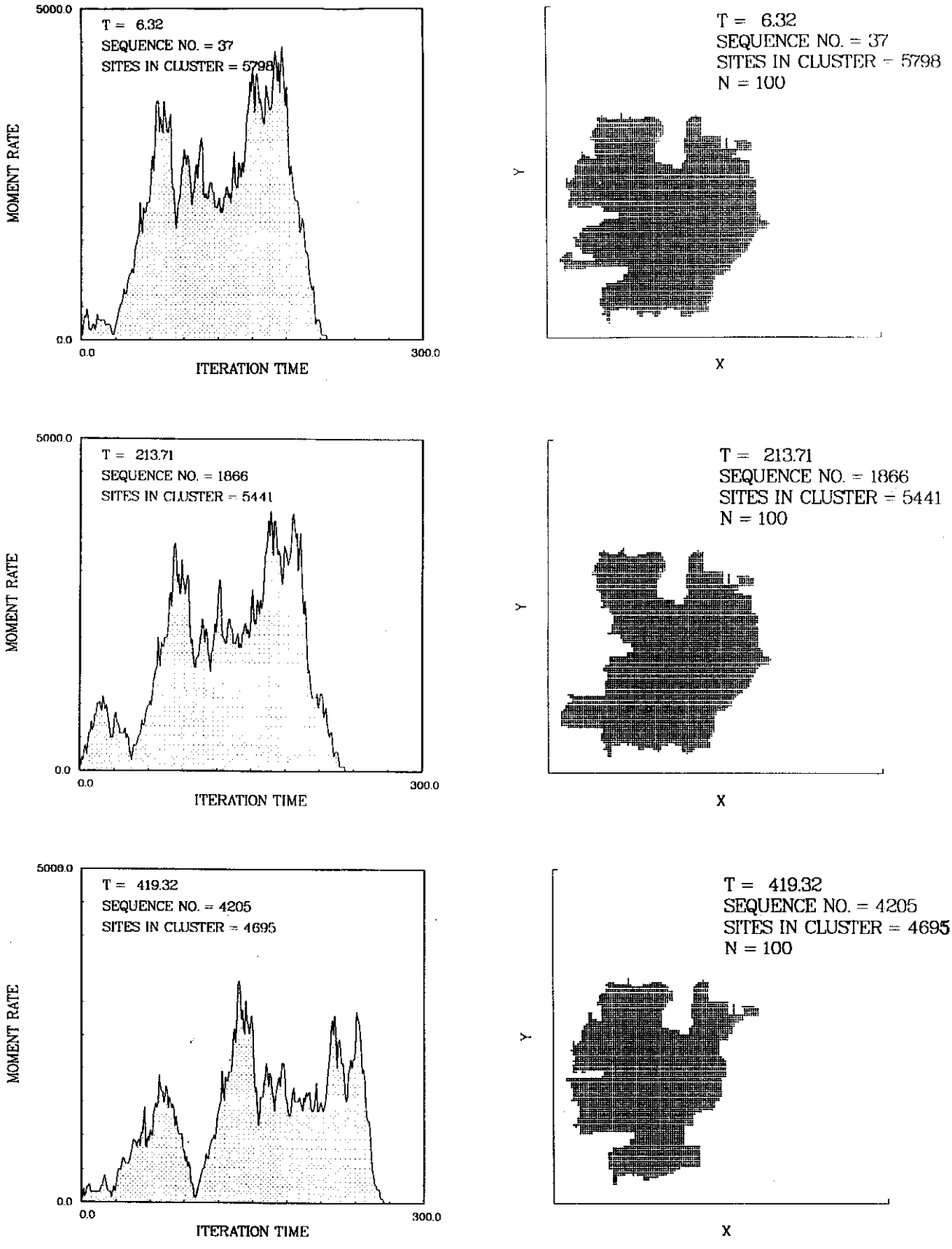

Fig. 4. Moment rate plotted against iteration (event) time (on left) for the first three large events shown in figures 2-3. Evolution of the spatial configuration of the events is associated with evolution of the moment rate function.

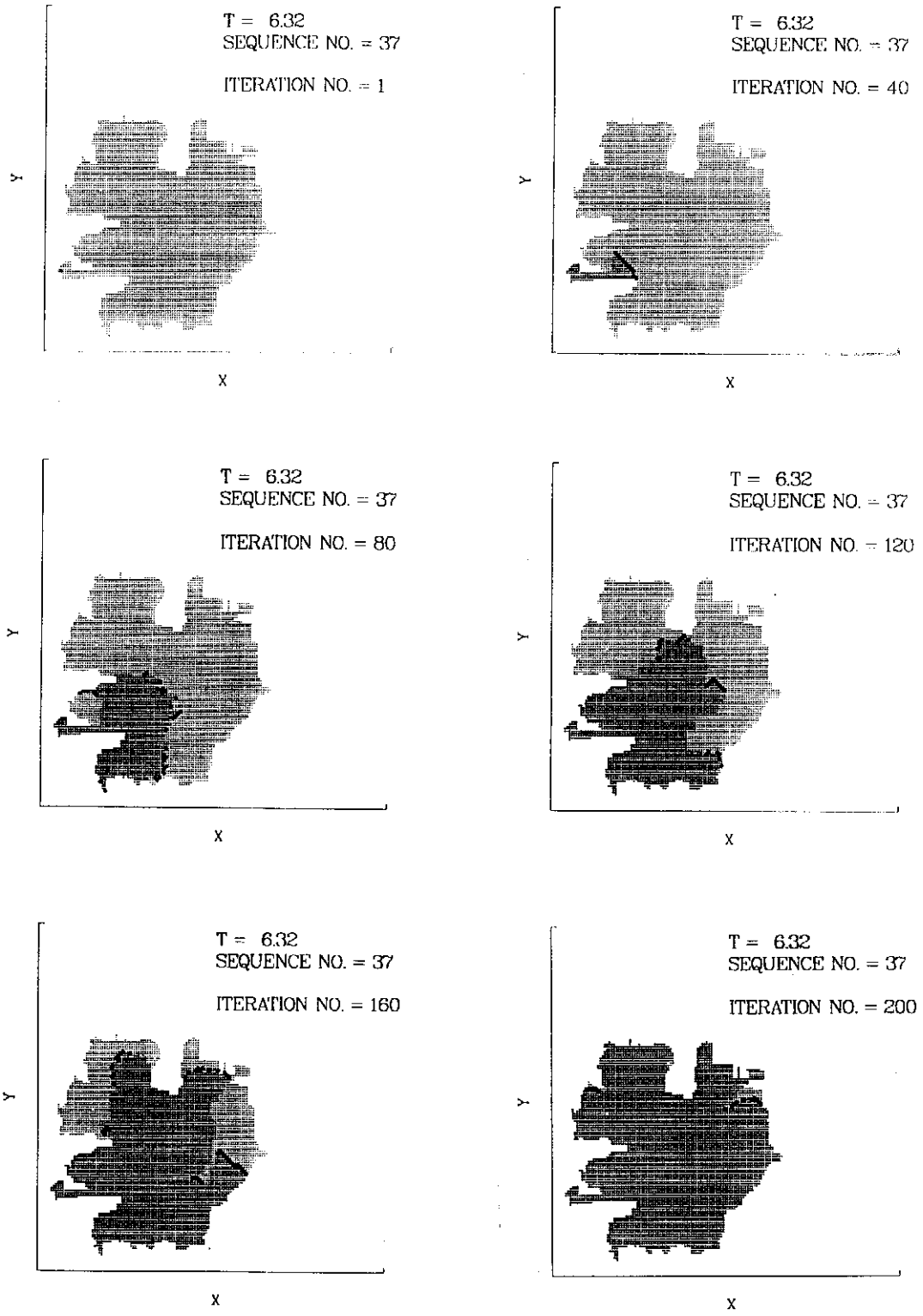

Fig. 5. Space-time pattern of failure (rupture) progression for the first large event that was also shown in figure 3-4. Initiation point (hypocenter) is shown at top left, other snapshots of failure are shown at intervals of 40 iteration time steps proceeding from upper left to bottom right. Lightest shading indicates sites that are yet to fail, darker shading indicates sites that have failed, and darkest shading are sites that are failing on the indicated iteration time step. In this case, the latter also constitute the rupture front, since in this model almost all sites fail only once.

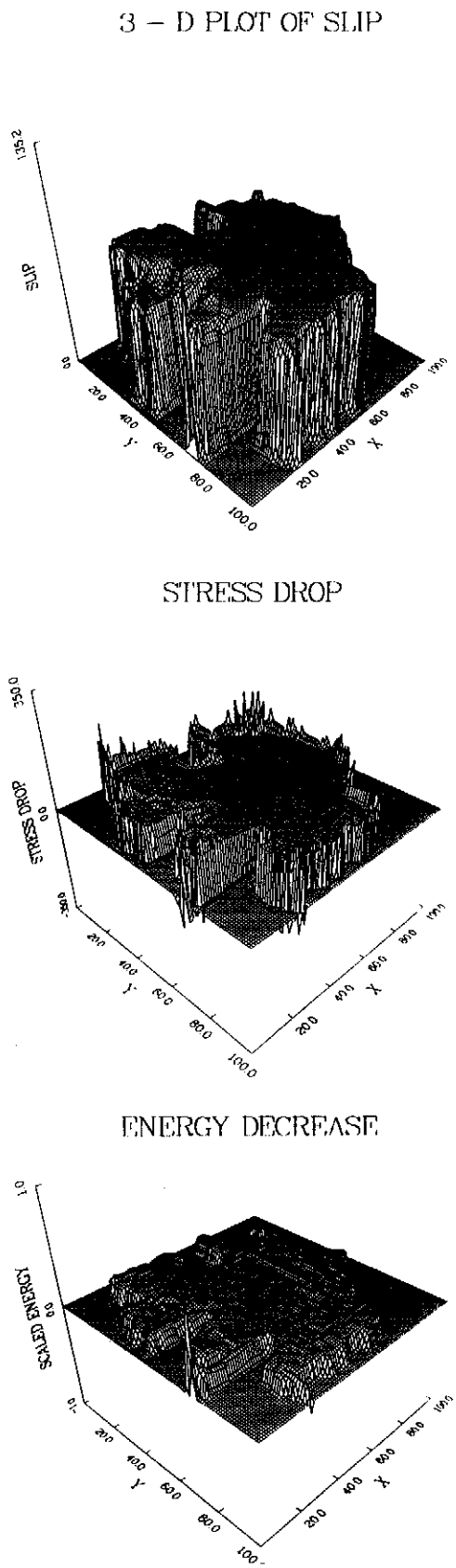

Fig. 6. (a) Top is three dimensional perspective plot of the slip in the first large event shown in figure 5. (b) Middle is plot of stress drop. (c) Bottom is energy decrease. Note that all quantities are nearly constant as a function of spatial position.

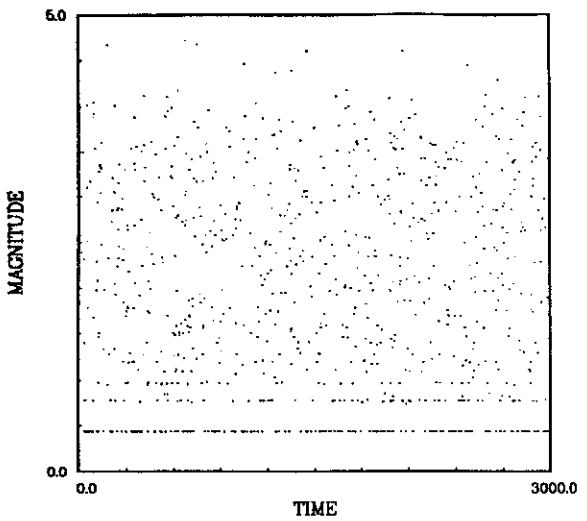

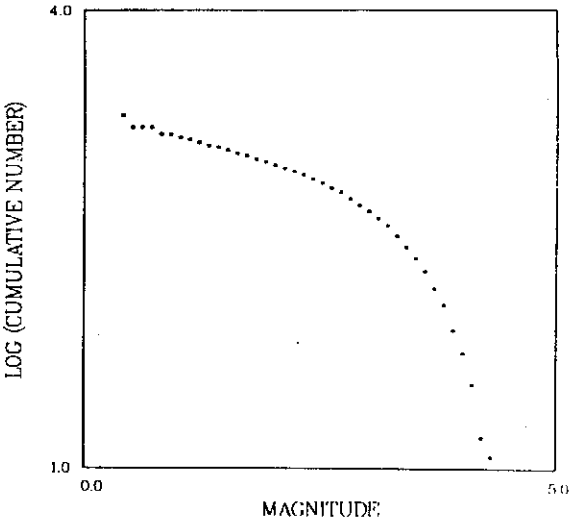

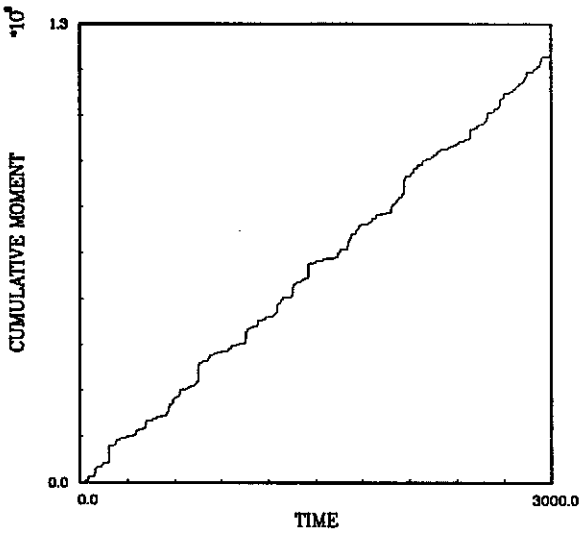

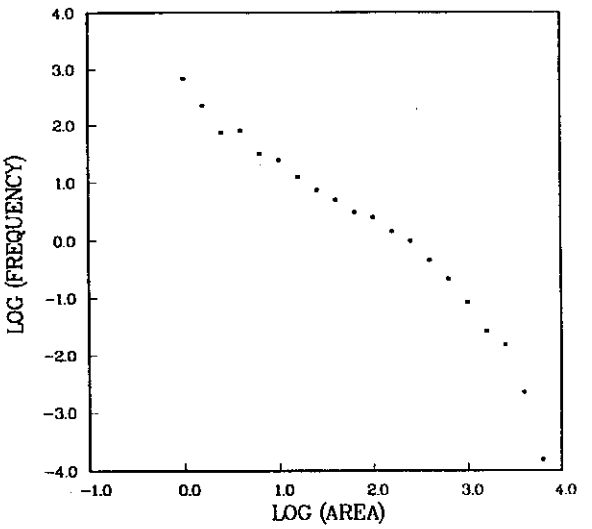

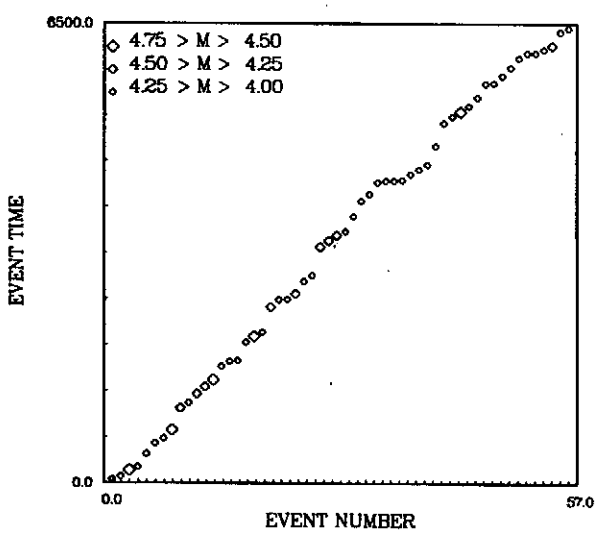

Fig. 7. Results from simulation with $K_C / K_L = 25$, $K_L = .04$. (a) Top left is magnitude-time plot of synthetic events, with magnitude as defined in the text. (b) Middle left is cumulative moment-time plot. (c) Bottom left is event time plotted against sequence number for the largest events shown in (a) and (b). (d) Top right is cumulative magnitude-frequency relation for all events. Unlike figure 2, the magnitude-log frequency relation is not well represented by a straight line. (e) Probability density for frequency of occurrence plotted against area of event. Again, these synthetic data are not well represented by a line (i.e., power law for frequency-area).

magnitudes where events with many failed sites are resolved into single isolated points. That the one-site events appear as a horizontal line is due to limitations in resolution of the laser printer. The first three largest magnitude events, near the top of the plot, are approximately equidistantly spaced in time, and are followed by a sequence of ~3 large events clustered more closely in time. These large events are examined in more detail below.

In figure 2, the left middle plot shows cumulative magnitude as a function of time, and resembles many such plots of real data (e.g., McNally, 1981). The left bottom plot shows the largest events in the form of a "recurrence plot" of event time in terms of event sequence number, similar to that commonly used to present Parkfield data (Bakun and McEvilly, 1984; see also Scholz, 1990, p. 246). Temporal clustering of the large events can be seen, implying that earthquake straight-line forecasting/ prediction, using time-predictable or slip-predictable ideas, is possible for only limited time intervals in this model. The top right plot is the cumulative number N of events as a function of magnitude (Gutenberg-Richter plot) for the events, and these simulation data conform to the relation:

$$\mathrm{Log}_{10}\, N = 5.1 - .85\, M \qquad (12)$$

The b value of .85 is not in agreement with the value near 1 observed in nature, because the observational data uses a relation between M and $\mathrm{Log}_{10}\, M_O$ different by a factor of 2/3. However, it may be significant that the relation between Log_{10} {Frequency} and Log_{10} {Area} has a slope (-1.89: lower right plot). Note that the "frequency" in this frequency-area plot is the probability density function for frequency, not the cumulative frequency. An observational-empirical value for this exponent of -2 is implied by the observational moment-magnitude scale. For the cumulative frequency, an observational value of -1 is found.

Fig. 3 shows the spatial configuration of the failed blocks for the first five largest events, as indicated along the top of figure 2 (top left). The events resemble one another closely. Gabrielov et al. (1994) and Herz and Hopfield (1995) have shown that a very similar model with a constant jump $J(\sigma_i) = (\sigma^F - \sigma^R) / K_T$ leads to strictly periodic events. For $K_C / K_L = 1$, it will be seen below that the stress transfer is small enough that the slip is very nearly spatially constant, similar to the periodic model, so that nearly periodic behavior is expected. For larger $K_C / K_L = 25$, the spatial distribution of slip in large events is more spatially heterogeneous, and the model shows less evidence of approximately periodic behavior. Self-organization is an intrinsic property of these models, and originates from the long-wavelength correlation of fluctuations. Patterns will emerge, persist for a period of time, then disappear to be replaced by new patterns. The events seen in figure 3 are reminiscent of characteristic earthquakes (Schwartz and Coppersmith, 1984), in which similar events will repeat at regular intervals for a period of time. The most famous example of this behavior is the Parkfield sequence (Bakun and McEvilly, 1984). Moreover, in the limit of weak coupling, the present slider block model becomes identical to a model which has been shown to demonstrate only periodic behavior (Gabrielov et al., 1994). This result suggests that segmentation on faults may be a result of the nonlinear dynamics, as well as the geometric configuration of the fault zone arising from bends and jogs in the fault (King and Nabelek, 1985).

Fig. 4 illustrates the analogue of the source-time moment rate function (left side) for the first three of these large events (right side). Each event develops as an avalanche of failed blocks that occur during a series of iteration sweeps through the lattice. The moment rate as a function of interation time is obtained by summing the slip produced by all the blocks that fail during each iteration sweep. This function is the analogue to the source-time function for real events. We remark that although our simulations involve massless blocks, there is a clear pattern of propagation across the lattice, at a local rupture velocity $v_r = 1$ grid unit per iteration sweep. Given a grid size, these results could in principle be scaled up to natural faults for comparison, although we do not pursue this farther here. From figure 4, both the spatial pattern of block failures and the moment rate function change with succeeding events. In particular, the area under the moment rate curve associated with the small "pre-shock", that is apparent at the beginning of the first event at top left, grows in importance until by the third event (bottom left) it represents a significant fraction of the total area under the curve associated with the "main event". A point to notice is the "jagged" temporal fluctuations in the moment rate functions, which are comparable to the mean value of the moment rate when averaged over time.

Another view of the source process is afforded by plots showing the time development of rupture during the event. Fig. 5 illustrates this process for the first large event, in which the lightly shaded region indicates all of the sites that eventually fail, the darker region represents the cumulative sites that have failed by the iteration sweep shown in the upper left of each panel. The darkest sites represent the sites that are failing on the indicated iteration sweep, and represent the rupture front. Beginning at the upper left, the rupture nucleation point can be seen as the dark site near the lower lefthand corner. The plot on the upper right is an early iteration time snapshot of the rupture front after 40 iteration time intervals. Rupture progression is documented at further iteration times of 80, 120, 160, and 200. It can be seen that the rupture process in this model is as suggested by the slip pulse model of Heaton (1990), in that a narrow region at the rupture front sweeps rapidly over sites on the fault, leaving slipped sites behind the rupture front locked again. Somewhat unlike the Heaton model, however, the rupture front is not necessarily a continuous line of slipping sites, but is quite irregular, sometimes consisting of only a very few sites. After about 200 iteration steps, slip on the model fault is complete.

Fig. 6 shows pseudo-three dimensional views of the slip (top), stress drop (middle), and energy decrease (bottom) for the first large event in the sequence, the same event as shown previously in figures 2-5. The distinguishing characteristic of all three plots is the spatially constant nature of the changes in slip, stress and energy. From the comments above, we expect to see some evidence of periodic behavior in a model where the slip during events is spatially homogeneous.

Fig.s 7-10 are a series of plots similar to figures 2, 4-6, but for a model in which $K_C / K_L = 25$ ($K_C = 1$, $K_L = .04$). In figure 7 top left, there is less evidence of temporal clustering than was seen in figure 2 top left. However, there are still a number of very large events similar to those seen for the previous case, and these events are the subject of the succeeding figures. Among obvious differences between figures 7 and 2, the "Parkfield recurrence plot" shown in the bottom left is evidently more linear than the corresponding plot in figure 2; the magnitude-frequency plot is not well represented by a relation of the form (12), unlike the result in figure 2; and the frequency-area relation is not so good a power law as that shown in figure 2, and has a lower average slope (about -1.6). In fact, the magnitude-frequency relation at top right of figure 7 is somewhat similar to that observed for isolated segments of major fault zones such as the Prince William sound section of the Alaska subduction zone (e.g., Scholz, 1990, p.188). This type of magnitude-frequency relation has been used to justify the characteristic earthquake model of earthquake recurrence along a fault.

Fig. 8 is analogous to figure 4 but for the first two large events in the magnitude-time plot in figure 7 ($K_C / K_L = 25$). This figure again suggests that segmentation can arise from dynamical causes. The source time (moment rate) functions in figure 8 are again calculated by summing the slip of each sliding block at a given iteration time. Unlike figure 4, however, the moment rate functions shown here are much smoother, having fluctuations that are only a small fraction of the value of the function averaged over iteration time. The reason for the difference is evidently associated with the larger value of K_C / K_L. K_C in equation (2) multiplies the nearest neighbor difference term, inducing a spatial smoothing of the slip deficit $\phi_i(t)$, so the sharp edges seen in the slip distribution of figure 6 are not present. The same statement applies to k_C and smoothing on $\phi(x,t)$ in (5). Spatially smoother slip deficit is observed to be associated with temporal smoothing in our simulations. We believe this implies that the states to which ϕ_i can jump are nearer together in state space. Spatial and temporal fluctuations are therefore damped, and the source time function is smoother.

Fig. 9 is a plot of the time development of the rupture for the first large event shown in figure 7. The first unstable site (hypocenter, or initiator site) is in the panel at upper left, and the sequence proceeds at 40 iteration-step intervals from left to right and top to bottom as in figure 5. The most obvious difference between the two figures (5 and 9) is that failure takes place only at the rupture front in figure 5, whereas there is a broad zone of failing sites behind the initial rupture front in figure 9. This broad zone is a result of the relatively large value of $K_C / K_L = 25$, indicating that the ratio of stress redistributed from the failed site to the stress lost by slip of the site, is large. A site can fail once, be loaded again by a failed neighbor to a large value of stress in excess of σ^F, and fail a subsequent time. In fact, the number of times a block can fail for large K_C / K_L is in principle unbounded, resulting in a spatially broad zone of failing sites. Models with large K_C / K_L have a large value of "stress conservation". The terminology is unfortunate, because energy can be conserved, not force and stress. Moreover, even in models in which stress is fully "conserved", it is essential that some stress be lost at the boundaries of the lattice, otherwise the average value of stress in the lattice will rise monotonically until it always exceeds the threshold σ^F.

Fig. 10 shows three dimensional perspective views of the slip, stress drop, and energy decrease for the event shown in figure 9. In contrast to figure 6, in which these quantitites are essentially constant over the area of failure, figure 10 indicates substantial spatial variation of slip, stress drop, and energy change, a result of the repeated and irregular pattern of failure for individual sites.

4 Implications and conclusions

Two important results from the foregoing are repeated and summarized in figure 11. On the left side top is the moment rate function, and on the bottom is the spatial distribution of slip, for the event with $K_C / K_L = 25$ in figures 8-10. On the right are the corresponding moment rate (top) and slip distribution (bottom) for the event with $K_C / K_L = 1$ in figures 4-6. Smoother source time functions are associated with spatially varying slip, whereas source time functions that fluctuate more strongly in time are associated with a slip distribution that has abrupt changes and sharp edges.

These numerical results may be compared with data describing the asperity model taken from the paper by Ruff (1983) and reproduced in figure 12. This figure describes results from two earthquakes, the 1964 Alaskan event (left), and the 1963 Rat Islands earthquake (right). At the top are long period seismograms (solid lines) together with fits (dashed lines) using long period synthetics that were used to obtain the moment rate functions (middle) for the events. At the bottom are the inferred spatial slip distributions for the events, which were obtained using assumptions about the space-time progression of rupture on the fault plane. According to these assumptions, the temporally smooth moment rate function for the Alaskan event is associated with a slip distribution that is nearly spatially constant. On the other hand, a moment rate function that fluctuates strongly in time is associated with spatially varying slip. This is the essence of the asperity model, in which

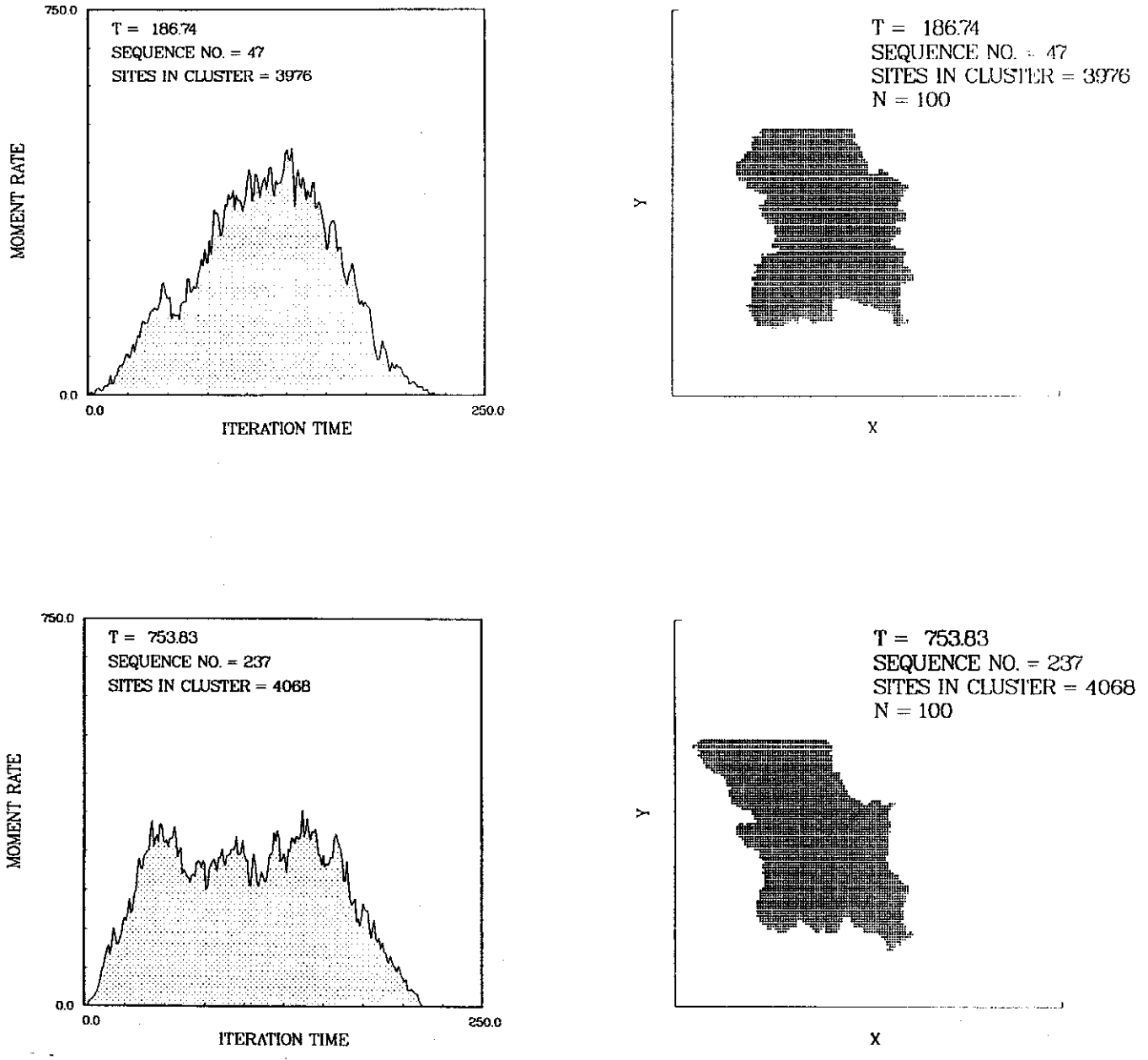

Fig. 8. Moment rate plotted agains iteration (event) time (on left) for the first two large events shown in figures 7 (top left) for the model with $K_C / K_L = 25$. Plot is analogous to figure 4. Evolution of the spatial configuration of events is associated with evolution of the moment rate function.

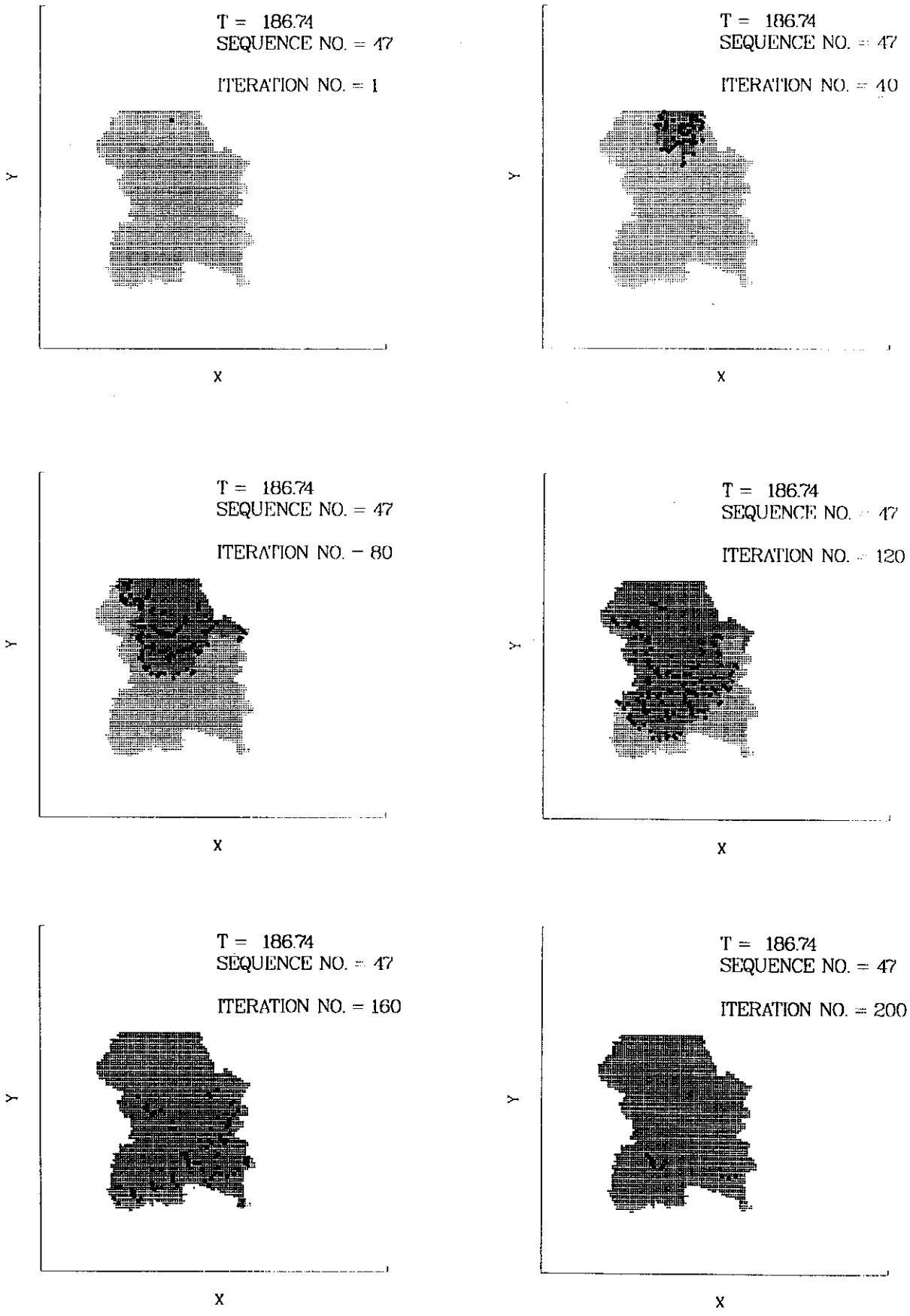

Fig. 9. Space-time pattern of rupture progression for the first large event that was shown in figure 8. Initiation point (hypocenter) is shown at top left, other snapshots of failure are shown at intervals of 40 iteration time steps proceeding from upper left to bottom right. Lightest shading indicates sites that are yet to fail, darker shading indicates sites that have failed, and darkest shading are sites that are failing on the indicated iteration time step. Only a few of the latter sites can be considered to constitute the rupture front, since this model, sites can be considerable amount of slip is occuring on previously ruptured sites.

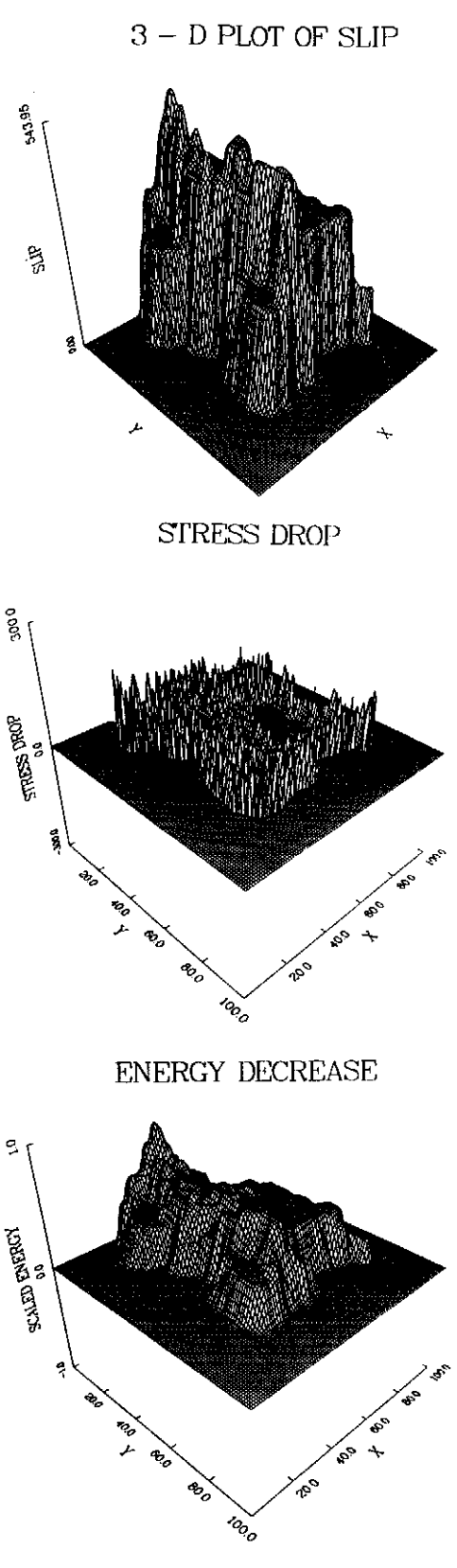

Fig. 10. (a) Top is three dimensional perspective plot of the slip in the first large event shown in figure 5. (b) Middle is plot of stress drop. (c) Bottom is energy decrease. Note that all quantities vary considerably with spatial position.

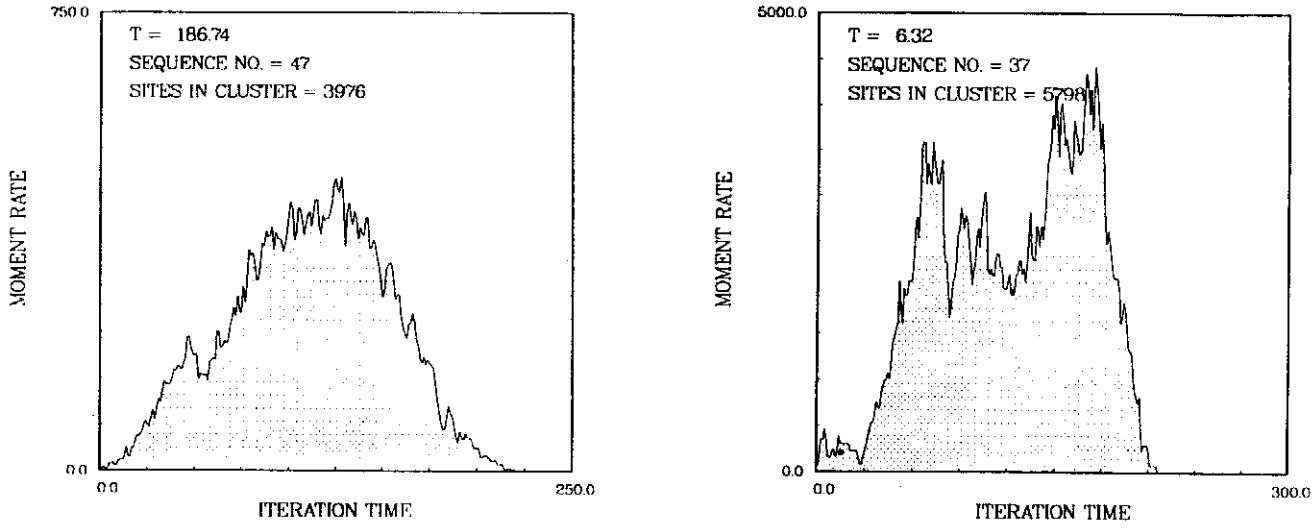

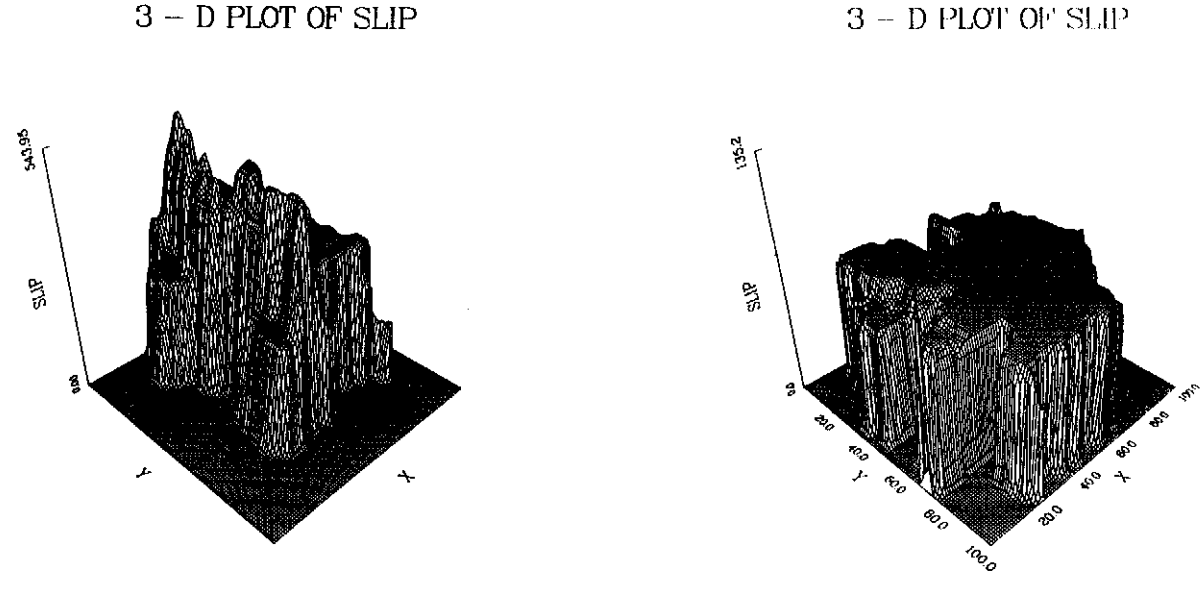

Fig. 11. Summary of results for model with (a) $K_C / K_L = 25$ (left) and (b) $K_C / K_L = 1$ (right). At top is the moment rate functions for the events, at bottom is the perspective plot of slip.

restricted areas on the fault have slip larger in magnitude than that which occurs over the bulk of the fault plane during the event.

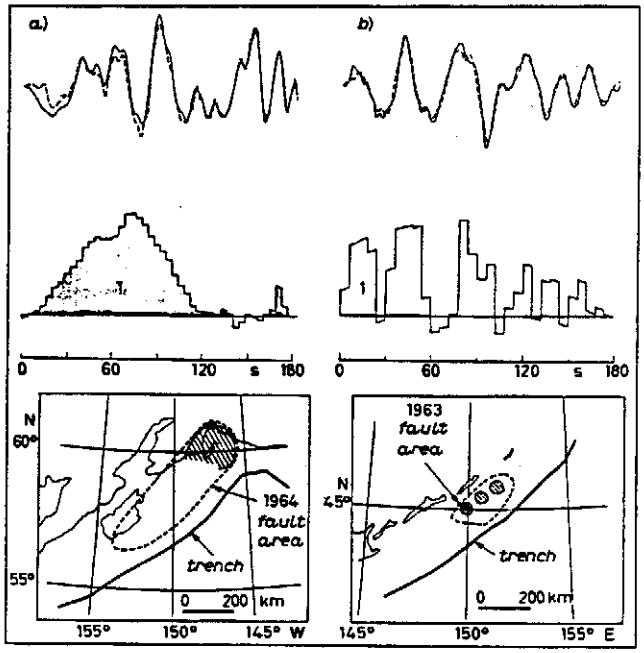

Fig. 12. Data and interpretation in terms of the asperity model for (a) the 1964 Alaskan earthquake (on the left) and (b) the 1963 Rat Islands earthquake (on the right). At top are observed (solid line) and synthetic (dashed line) seismograms for the events. Seismogram for Alaska is from La Paz, Bolivia, and for Rat Islands, Pasadena, CA. Middle plots show moment rate source time functions for the events obtained by matching synthetics to the data for a number of stations (see Ruff, 1983). At bottom are cartoons showing the slip patterns obtained, assuming that rupture velocity and directivity are constant, so that the amount of fault area ruptured per unit time is constant *(after Ruff, 1983)*.

The results of figures 11 and 12 are an interesting paradox. To the extent that results from the simple toy model may apply to real earthquakes, figure 11 indicates that temporally smooth source time functions are associated with spatially varying slip. However, results obtained from source time functions for the Alaskan earthquake, shown in figure 12, are thought to imply relatively constant slip. Additionally, figure 11 implies that strong temporal fluctuations in the moment rate function are associated with spatially constant slip in the toy model, unlike the Rat Island earthquake data shown in figure 12. These differences have motivated us to examine the assumptions that underlie the observational results. For the moment, we take as given the techniques by which long period seismograms can be used to obtain the moment rate functions. In going from the moment rate functions to the slip distributions, however, a critical assumption is often made whose validity may be difficult to prove under general conditions. Specifically, the assumption used in obtaining the results in figure 12 is that rupture velocity and directivity during the earthquake is constant, or equivalently, that the amount of fault plane ruptured in a given interval is constant (Beck and Ruff, 1984, 1985; Beck and Christensen, 1991; Schwartz and Ruff, 1985, 1987). If this were true in nature, smooth moment rate functions would certainly be associated with nearly constant slip, whereas strongly fluctuating moment rate functions would imply strong variations in slip. Variations in slip are then interpreted as providing evidence for large variations in "strength". Other data that may support the existence of strength-related asperties have been presented by Dmoska and Lovison (1992); Engdahl et al. (1989); and Schwartz et al (1989).

The simple toy model provides a counter example to these assumed properties of the rupture process. It can be seen in figures 5 and 9 that rupture velocity and directivity are not constant. Moreover, in both the case with $K_C / K_L = 1$ and that with $K_C / K_L = 25$, the strength (threshold σ^F) is constant. For our models, variations in the elastic coupling are the cause of spatial variations in the slip. Whether this is also true in nature is at the present unknown, but this result at the least provides a new conceptual model to be tested by data.

The contrast between the rupture patterns in figures 5 and 9, leads us to speculate about the possibility of a rupture model complementary to the Kostrov crack-like model and the Heaton pulse model. In both models, rupture proceeds outward from an initial nucleation point, the difference lying in the healing process behind the rupture front. In the former, no healing occurs until the rupture front progression comes to an end, whereas in the latter, healing at a point takes place immediately after the rupture front passes. We propose a third model, whose principal difference is that rupture proceeds outward from several sites nearly simultaneously, coalescing into a large slipped patch on the fault. Healing occurs as in the Heaton model, soon after the rupture front passes by. The nearly simultaneous appearance of several failing patches would be possible under the conditions that (1) the rupture velocity is less than the shear wave speed at which the shear stress is transmitted across the fault plane; and (2) stress on the fault is everywhere near the threshold, implying that a finite failure correlation length exists. This "coalescence" model has the additional property that the scaling statistics (power law exponents) are universal, and do not depend on details of the fault plane geometry, plate velocities, or other details, properties that seem to be true for b-values and p-values of seismicity distributions. These scaling powers are those for mean field spinodal dynamics (Rundle et al., 1995a).

The coalescence model for nucleation can occur in any system having long range interactions (Monette and Klein, 1993), or equivalently, in a slider block model having a large value for K_C / K_L This ratio can be shown to depend on the blocking size a, and the characteristic fault length λ. Using the definitions (6)-(7), and assuming that $T(\mathbf{r}) \sim 1/|\mathbf{r}|^3$ we find that asymptotically:

$$K_L \sim -\int_a^{\lambda} T(r)\, d^2r \sim (1/a) - (1/\lambda) \quad (13)$$

$$K_C \sim 1/(2a^2) \int_a^{\lambda} T(r)\, r^2\, d^2r \sim (\lambda - a)/2a^2 \quad (14)$$

so that:

$$K_C / K_L \sim \lambda / 2a \quad (15)$$

Recall that this estimate for K_C / K_L has been derived assuming a planar fault, and a perfectly elastic material. The small-scale block size is a result of physical processes that violate either of these assumptions. Estimates for the block size a for a fault zone can range from the inelastic fault thickness of tens to hundreds of meters (Rundle, 1993), up to characteristic nonplanar fault jog lengths of kilometers to tens of kilometers or more (e.g., Scholz, 1990). This would imply that large faults, with $\lambda >> a$ should be characterized by large ratio K_C / K_L. However, as discussed in connection with (5)-(7), there are physical reasons to expect that the real stress Green's function may not be of infinite range, but because of local factors, might have a screening length $1/\alpha$. In that case, $K_C \sim e^{-\alpha a} / a^2\alpha$, $K_L \sim \alpha\, \Gamma(3)$, where Γ is the Gamma function, and assuming $\lambda >> a$. The ratio K_C / K_L is then approximately:

$$K_C / K_L\, e^{-\alpha a} / a^2\alpha^2 \quad (16)$$

If $\alpha \sim 1/a$, K_C / K_L will be of order 1. Though the physical existence of a small scale block size and an elastic cutoff is currently the subject of considerable debate, it has nevertheless been argued that the earth may behave this way (e.g., Aki, 1987; Rundle, 1993; Rundle and Klein, 1993). The conclusion is that the ratio K_C/K_L appropriate for a given fault depends on the physical structure of the fault, as well as its overall size. Here we observe that a small ratio corresponds to what is called an 'asperity', and a large ratio corresponds to what is called a 'uniform' strength frictional surface (no 'asperity'). There need not be a single value of K_C/K_L for the entire earth, but instead the value would differ depending on the fault structure.

To summarize our main results, we examined a simple toy slider block model and find that variations in slip distribution are related to variations in elastic coupling, so that variations in threshold strength are not needed to reproduce the phenomena observed in nature. Moreover, the rupture velocity and directivity for large model events are not constant. These results do not support the usual assumptions made for interpreting long period seismograms in terms of slip distributions for real earthquakes. Our results also suggest that the nonlinear dynamics of the model can give rise to an apparent segmentation having a dynamical origin, in contrast to the more common model of segmentation arising from the geometric configuration of the fault.

Acknowledgements. JBR would like to acknowledge support from NASA contract NAG5-2353 to the Cooperative Institute for Research in Environmental Sciences at the University of Colorado in Boulder, Colorado. The authors would also like to acknowledge a valuable critical review by J.R. Rice.

References

Aki, K., Magnitude-frequency relations for small earthquakes: A clue to the origin of f_{max} of large earthquakes, *J. Geophys. Res.*, 92, 1349-1355, 1987.

Allen, M.P. and D.J. Tildsley, *Computer Simulations of Liquids*, Clarendon Press, Oxford, 1987.

Amit, D.J., *Field Theory, the Renormalization Group, and Critical Phenomena*, World Scientific, Philadelphia, 1984.

Arrowsmith, D.K. and C.M. Place, *An Introduction to Dynamical Systems*, Cambridge University Press, Cambridge, U.K., 1991.

Bak, P. and C. Tang, Earthquakes as a self-organized critical phenomenon, *J. Geophys. Res.*, 94, 15635-15638, 1989.

Bakun, W. and T.V. McEvilly, Recurrence models and Parkfield, California, earthquakes, *J. Geophys. Res.*, 89, 3051-3058, 1984

Beck, S.L. and L.J. Ruff, The rupture process of the great 1979 Colombia earthquake: Evidence for the asperity model, *J. Geophys. Res.*, 89, 9281-9291, 1984.

Beck, S.L. and L.J. Ruff, The rupture process of the 1976 Mindanao earthquake, *J. Geophys. Res.*, 90, 6773-6782, 1985.

Beck, S.L. and D.H. Christensen, Ruture process of the February 4, 1965, Rat Islands earthquake, *J. Geophys. Res.*, 96, 2205-2221, 1991.

Ben-Zion, Y. and J.R. Rice, Earthquake failure sequences along a cellular fault zone in a 3D elastic solid containing asperity and non-asperity regions, *J. Geophys. Res.*, 98, 14109-14131, 1993.

Binder, K., *Monte Carlo Methods in Statistical Physics*, vol. 7 of *Topics in Current Physics*, Springer-Verlag, Berlin, 1986.

Binder, K., *Applications of the Monte Carlo Method in Statistical Mechanics*, vol. 36 of *Topics in Current Physics*, Springer-Verlag, Berlin, 1987.

Burridge, R. and L. Knopoff, Model and theoretical seismicity, *Bull. Seism. Soc. Am.*, 57, 341-371, 1967.

Carlson, J.M and J.S. Langer, Properties of earthquakes generated by fault dynamics, *Phys. Rev. Lett.*, 62, 2632-2635, 1989.

Dmowska, R. and L. Lovison, Influence of asperities along subduction interfaces on the stressing and seismicity of adjacent areas, *Tectonophysics*, 211, 23-41, 1992.

Engdahl, E.R., S. Billington, and C. Kisslinger, Teleseismically recorded seismicity before and after the May 7, 1986 Andreanof Islands, Alaska, earthquake, *J. Geophys. Res.*, 94, 15481-15498, 1989.

Feynman, R.P. and A.R. Hibbs, *Quantum Mechanics and Path Integrals*, McGraw-Hill, New York, 1965.

Gabrielov, A., W. Newman and L. Knopoff, Lattice models of failure: Sensitivity to the local dynamics, *Phys. Rev. E*, 50, 188-197, 1994.

Haberman, R.E., Consistency of teleseismic reporting since 1963, *Bull. Seism. Soc. Am.*, 72, 93-111, 1982.

Heaton, T., Evidence for and implications of self-healing pulses of slip in earthquake rupture, *Phys. Earth and Planet. Int.*, 64, 1-20, 1990.

Hopfield, J.J., Neurons, dynamics and computation, *Physics Today*, 47, 40-46, 1994.

Herz, A.V.M. and J.J. Hopfield, Rapid phase locking in coupled integrate-and-fire neurons, preprint, 1995.

Kanamori, H, Global seismicity, pp. 596-608 in *Earthquakes: Observation, Theory and Interpretation*, Course LXXXV, Proc. Intl. School of Physics "Enrico Fermi", the Italian Physical Society, North Holland, Amsterdam, 1983.

Kanamori, H., Mechanics of Earthquakes, *Ann. Rev. Earth Planet. Sci.*, 21, 1993.

Kanamori, H. and D.L. Anderson, Theoretical basis for some empirical relations in seismology, *Bull. Seism. Soc. Am.*, 65, 1073-1095,1975.

King, G.C.P. and J. Nabelek, Role of fault bends in the initiation and termination of earthquake rupture*cience*, 228, 984-987, 1985.

Kostrov, BV, Self similar problems of propagation of shear cracks, *J. Appl. Mech.*, 28, 1077-1087, 1964.

Lay, T., H. Kanamori, and L. Ruff, The asperity model and the nature of large subduction zone earthquakes, *Earthquake Prediction Research*, 1, 3-71, 1982.

Ma, S.-K., *Statistical Mechanics*, World Scientific, Philadelphia, PA, 1985.

Ma, S.-K., *Modern Theory of Critical Phenomena*, Benjamin-Cummings, Reading MA, 1976.

McNally, K.C., Plate subduction and prediction of earthquakes along the Middle America Trench, in *Earthquake Prediction, An International Review*, AGU monograph 4, American Geophysical Union, Washington, DC, 1981.

Monette, L. and W. Klein, Spinodal nucleation as a coalescence process, *Phys. Rev. Lett.*, 68, 2336-2339, 1992.

Mouritsen, O.G., in *Computer Studies of Phase Transitions and Critical Phenomena*, Springer-Verlag, Berlin, 1984.

Nakanishi, H., Cellular automaton model of earthquakes with deterministic dynamics, *Phys. Rev. A*, 43, 6613-6621, 1990.

Narkounskaia, G., J. Huang and D.L. Turcotte, Chaotic and self-organized critical behavior of a generalized slider block model, *J. Stat. Phys.*, 67, 1151-1183, 1992.

Olami, Z., H.J.S. Feder, and K Christensen, *Phys. Rev. Lett.*, 68, 1244-1247, 1992 (comment by W. Klein and J.Rundle, *Phys. Rev. Lett.*, 71, 1288-1289, 1993)

Pacheco, J.F., C.H. Scholz and L.R. Sykes, Changes in frequency-size relationship from small to large earthquakes, *Nature*, 355, 71-73, 1992.

Richter, C.F., *Elementary Seismology*, W.H. Freeman, San Francisco, 1958.

Ruff, L.J., Fault asperities inferred from seismic body waves, pp. 251-276, in *Earthquakes: Observation, Theory and Interpretation*, Course LXXXV, Proc. Intl. School of Physics "Enrico Fermi", the Italian Physical Society, North Holland, Amsterdam, 1983.

Rundle, J.B., A physical model for earthquakes: 1, Fluctuations and interactions, *J. Geophys. Res.*, 93, 6237-6254, 1988.

Rundle, J.B., A physical model for earthquakes: 3, Thermodynamical approach and its relation to nonclassical theories of nucleation, *J. Geophys. Res.*, 94, 2839-2855, 1989.

Rundle, J.B., Magnitude frequency relations for earthquakes using a statistical mechanical approach, *J. Geophys. Res.*, 98, 21943-21949, 1993.

Rundle, J.B. and D.D. Jackson, Numerical simulation of earthquake sequences, *Bull. Seism. Soc. Am.*, 67, 1363-1378, 1977.

Rundle, J.B. and W. Klein, Nonclassical nucleation and growth of cohesive tensile cracks, *Phys. Rev. Lett.*, 63, 171-174, 1989.

Rundle, J.B. and W. Klein, Nonlinear dynamical models for earthquakes and frictional sliding: An overview, *Proc. 33rd Symposium Rock Mech.*, A.A. Balkema, Rotterdam, 1992.

Rundle, J.B. and W. Klein, Scaling and critical phenomena in a class of slider block cellular automaton models for earthquakes, *J. Stat. Phys.*, 72, 405-412, 1993.

Rundle, J.B. and D.L. Turcotte, New directions in theretical studies of tectonic deformation: A survey of recent progress, in *Contributions of Space Geodesy to Geodynamics: Crustal Dynamics*, ed. D.E. Smith and D.L. Turcotte, Geodynamics Ser. Vol. 23, AGU, Washington, DC, 1993.

Rundle, J.B., J. Ross, G. Narkounskaia, and W. Klein, Earthquakes, self-organization, and critical phenomena, *J. Stat. Phys.*, submitted, 1995a.

Rundle, J.B., W. Klein and D.L. Turcotte, Observation of Boltzmann fluctuations in massless slider block simulations, *Santa Fe Institute Series in Complexity* , in press, 1995b.

Rundle, J.B. and W. Klein, New ideas about the physics of earthquakes, *AGU Quadrennial report to the IUGG and Rev. Geophys. Space Phys.*, in press, 1994.

Sahimi, M., M.C. Robertson, and C.G. Sammis, Fractal distribution of earthquake hypocenters and its relation to fault patterns and percolation, *Phys. Rev. Lett.*, 70, 2186-2189, 1993.

Schulman, L.S., *Techniques and Applications of Path Integration*, John Wiley, New York, 1981.

Schwartz, D.P. and K.J. Coppersmith, Fault behavior and characteristic earthquakes: Examples from the Wasatch and San Andreas faults, *J. Geophys. Res.*, 89, 5681-5698, 1984.

Schwartz, S.Y. and L.J. Ruff, The 1968 Tokachi-Oki and the 1969 Kurile Islands earthquakes: Variability in the rupture process, *J. Geophys. Res.*, 90, 8613-8626, 1985.

Schwartz, S.Y. and L.J. Ruff, Asperity distribution and earthquake occurrence in the southern Kurile Islands arc, *Phys. Earth Planet. Int.*, 49, 54-77, 1987

Scholz, C.H., *The Mechanics of Earthquakes and Faulting*, Cambridge University Press, Cambridge, U.K., 1990.

Schwartz, S.Y., J.W. Dewey and T. Lay, Influence of fault plane heterogeneity on the seismic behavior in the southern Kurile Islands arc, *J. Geophys. Res.*, 94, 5637-5649, 1989.

Senatorski, P., *Fault Zone Dynamics Evolution Patterns*, Ph.D. Dissertation, Geophysical Institute of the Polish Academy of Sciences (Polska Akademia Nauk, Instytut Geofizyki), Warsaw, 1993.

Smale, S., Differentiable dynamical systems, *Bull. Amer. Math. Soc.*, 73, 747-817, 1967.

Stauffer, D. and A. Aharony, *Introduction to Percolation Theory*, Taylor and Francis, London, 1992.

Yeomans, J.M., *Statistical Mechanics of Phase Transitions*, Clarendon Press, Oxford, 1992.